Review Article

The physical and biological basis of quantitative parameters derived from diffusion MRI

Gavin P Winston

Epilepsy Society MRI Unit, Department of Clinical and Experimental Epilepsy, UCL Institute of Neurology, London, UK

Corresponding to: Dr Gavin P Winston. UCL Institute of Neurology (Box 29), Queen Square, London, WC1N 3BG, UK. Email: g.winston@ucl.ac.uk.

Abstract: Diffusion magnetic resonance imaging is a quantitative imaging technique that measures the underlying molecular diffusion of protons. Diffusion-weighted imaging (DWI) quantifies the apparent diffusion coefficient (ADC) which was first used to detect early ischemic stroke. However this does not take account of the directional dependence of diffusion seen in biological systems (anisotropy).

Diffusion tensor imaging (DTI) provides a mathematical model of diffusion anisotropy and is widely used. Parameters, including fractional anisotropy (FA), mean diffusivity (MD), parallel and perpendicular diffusivity can be derived to provide sensitive, but non-specific, measures of altered tissue structure. They are typically assessed in clinical studies by voxel-based or region-of-interest based analyses.

The increasing recognition of the limitations of the diffusion tensor model has led to more complex multi-compartment models such as CHARMED, AxCaliber or NODDI being developed to estimate microstructural parameters including axonal diameter, axonal density and fiber orientations. However these are not yet in routine clinical use due to lengthy acquisition times.

In this review, I discuss how molecular diffusion may be measured using diffusion MRI, the biological and physical bases for the parameters derived from DWI and DTI, how these are used in clinical studies and the prospect of more complex tissue models providing helpful micro-structural information.

Key Words: Diffusion MRI; diffusion weighted MRI; diffusion tensor imaging; white matter

Submitted Nov 13, 2012. Accepted for publication Dec 19, 2012.

DOI: 10.3978/j.issn.2223-4292.2012.12.05

Scan to your mobile device or view this article at: http://www.amepc.org/qims/article/view/1315/1771

Introduction

Diffusion magnetic resonance imaging (MRI) is fundamentally a quantitative imaging technique. Unlike T_1 and T_2 mapping approaches which are dependent upon the magnetic field strength, diffusion-derived measures should be comparable between centers. Diffusion MRI measures a single phenomenon - the dephasing of proton spins in the presence of a spatially-varying magnetic field ("gradient") (1) - through non-invasive *in vivo* imaging. Mathematical models of the underlying tissue enable the determination of parameters describing the tissue microstructure. Diffusion MRI can be applied to any body part but is most frequently used for neuroimaging which is the focus of this review.

First I discuss the concept of molecular diffusion and how it may be measured using diffusion MRI. Then I review diffusion-weighted imaging and the apparent diffusion coefficient before considering the various metrics that can be derived from diffusion-tensor imaging, the biological sources of anisotropic diffusion and how to extract and interpret these parameters in clinical studies. Finally, I discuss more complex tissue models that may be employed to quantify microstructural parameters. This review does not summaries the extensive clinical studies in the area, nor does it address technical features such as hardware, acquisition schemes or imaging artifacts.

Diffusion and its measurement

Molecular diffusion

Any particle at a temperature above absolute zero possesses

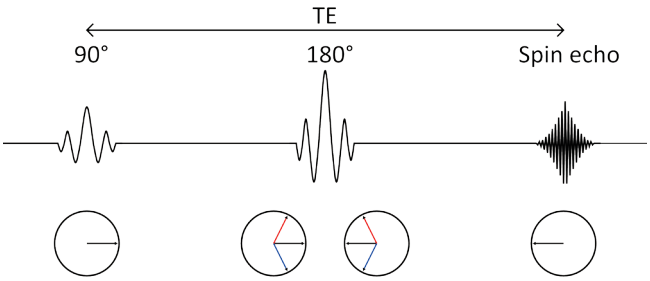

Figure 1 Spin echo NMR sequence. The 90 degree RF pulse produces coherent transverse magnetization (first circle). The spins begin to dephase due to magnetic field inhomogeneities (red, blue and black arrows in the second circle). The 180 degree pulse reverses the phase dispersal (third circle). The spins then rephase and produce an echo (fourth circle)

thermal energy that manifests as random movement ("molecular diffusion"). In the presence of a concentration gradient, the net flux of particles from high to lower concentration was described by Fick's First Law in 1855 (2):

$$\mathbf{J} = D\nabla C \qquad [1]$$

where J is the diffusive flux, D is the diffusion coefficient and C is the particle concentration.

Einstein recognized that diffusive mixing occurs in the absence of a concentration gradient ("self diffusion"). By considering the conditional probability distribution of a group of particles after a time t, the mean squared displacement after a given time is proportional to the diffusion coefficient (Einstein's relationship) (3):

$$\langle x^2 \rangle = 2Dt \text{ or } \langle \mathbf{r}^2 \rangle = 6Dt \qquad [2]$$

where $\langle x^2 \rangle$ is the mean squared displacement of the particle (in one dimension) (or $\langle \mathbf{r}^2 \rangle$ in three dimensions), D is the diffusion coefficient and t is the diffusion time.

Measurement of diffusion: NMR

A standard spin echo sequence is shown in *Figure 1* (4). The 90 degree radiofrequency (RF) pulse rotates the magnetization vector into the horizontal plane. Spins precess at the Larmor frequency but begin to dephase due to magnetic field inhomogeneities leading to signal decay. The 180 degree pulse reverses the phase dispersal enabling the spins to rephase and produce an echo.

The addition of two gradient pulses that induce a spatially dependent phase shift makes this sequence sensitive

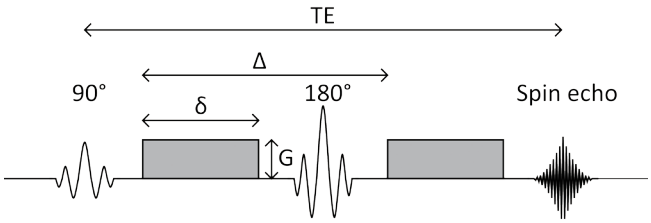

Figure 2 Pulsed gradient spin echo NMR sequence. The spin echo sequence is modified by the addition of two gradient pulses (grey blocks) which induce and then reverse a spatially-dependent phase shift

to the effects of diffusion (*Figure 2*) (5). For static (non-diffusing) spins, the phase shifts induced by two opposing gradients cancel. However for moving (diffusing) spins, the cancellation is incomplete leading to residual phase dispersal and further signal attenuation. The degree of signal attenuation is given by the Stejskal-Tanner equation:

$$\ln\left(\frac{S_{G,\Delta,\delta}}{S_0}\right) = -\gamma^2 G^2 \delta^2 \left(\Delta - \frac{\delta}{3}\right) D \qquad [3]$$

where $S_{G,\Delta,\delta}$ and S_0 are the echo signal in the presence and absence of the diffusion gradients, γ is the gyromagnetic ratio, G is the gradient amplitude, Δ is the pulse separation, δ is the pulse duration and D the diffusion coefficient. These parameters are usually combined into a single parameter known as the b-factor where:

$$b = \gamma^2 G^2 \delta^2 \left(\Delta - \frac{\delta}{3}\right) \qquad [4]$$

Measurement of diffusion: MRI

Diffusion NMR experiments can be extended to three dimensions by applying diffusion-weighting gradients in any direction (*Figure 3*). The Stejskal-Tanner equation only remains valid for tissues in which diffusion shows no directional dependence and it neglects the interaction between imaging and diffusion gradients when these are applied in different directions. In practice, signal attenuation must be calculated used diffusion-modified Bloch equations (6) and these interactions are all included in the b-factor.

Clinical scans are typically acquired using echo-planar imaging (EPI) in which all the data points necessary to reconstruct the image are sampled after a single 90-180 pair of RF pulses (7). However, due to the low bandwidth in the phase encode direction this sequence is very susceptible to

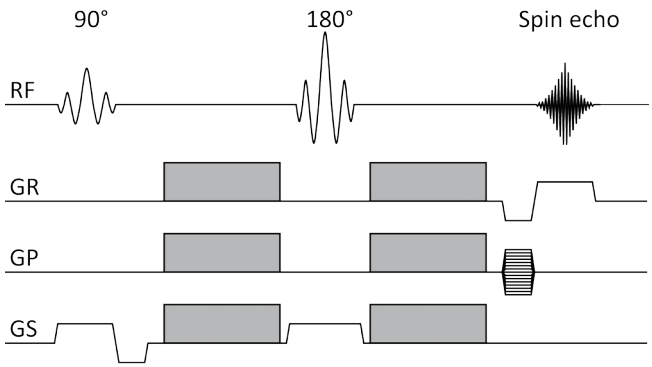

Figure 3 Diffusion-weighted spin echo MRI sequence. RF shows the 90 and 180 degree pulses, GR is the readout gradient (typically x-direction, left-right), GP is the phase-encoding gradient (typically y-direction, antero-posterior) and GS is the slice-select gradient (typically z-direction, supero-inferior). The diffusion gradients (grey blocks) can be applied as any combination of these directions

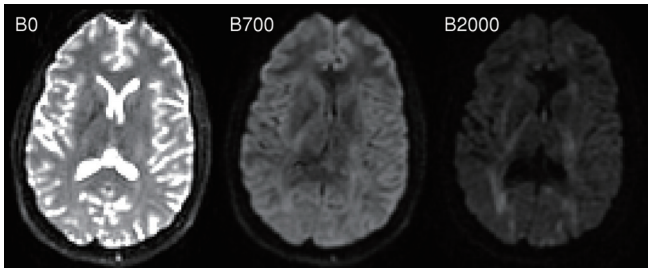

Figure 4 Diffusion-weighted imaging with different degrees of weighting. The image on the left is a T2-weighted EPI image with no diffusion-weighting (b=0 s·mm^{-2}), the middle image has a modest degree of diffusion-weighting (b=700 s·mm^{-2}) and the right hand image has a high degree of diffusion-weighting (b=2,000 s·mm^{-2}). The diffusion gradients have been applied in the x-direction (left-right). Note the high attenuation in CSF where the diffusion coefficient is high and the lower attenuation in white matter structures such as the internal capsule running perpendicular to the diffusion gradient direction

off-resonance effects such as magnetic field inhomogeneity, local susceptibility gradients and chemical shift. Subject motion and eddy currents induce further artifacts. Imaging artifacts are reviewed elsewhere (8) and may be ameliorated using parallel imaging, other pulse sequences or alternative k-space trajectories (9).

Diffusion weighted imaging (DWI)

The echo signal in a typical spin echo sequence (*Figure 3*) combines T_2 and diffusion-weighting (with only negligible T_1 weighting):

$$M = M_0 \exp\left(-\frac{TE}{T_2}\right)\exp(-bD) \quad [5]$$

where M is the measured echo signal and M_0 is the signal after the 90 degree RF pulse.

By measuring the signal at two different b-values the effects of T_2 decay can be removed leaving just the diffusion-weighted attenuation. In particular with a diffusion-weighted scan and a non-diffusion weighted scan acquired with the same TE, we see by combining equations [3] and [4] that

$$\ln\left(\frac{S_b}{S_0}\right) = -bD \quad [6]$$

Thus it is possible to determine the diffusion coefficient D in each voxel of the image. A more accurate estimate can be obtained via linear regression with a series of DWI of different b-values (*Figure 4*) (10). However with typical diffusion times of 30 ms on an MRI scanner and a diffusion coefficient of water at 37 ℃ of 3.0×10^{-3} mm^{2}s^{-1} the diffusion distance of around 20 μm exceeds the size of structures such as cells. Thus barriers such as cell membranes hinder free diffusion and the signal attenuation is also modulated by other factors including perfusion. The diffusion coefficient term D is therefore replaced by the apparent diffusion coefficient *ADC* (11), typically around 0.8×10^{-3} mm^{2}s^{-1} in white matter.

ADC was initially shown to be a sensitive early indicator for ischemic stroke in cats (12) and subsequently in humans (13). The calculation of this quantitative parameter is critical as "bright" areas on a raw diffusion-weighted image (representing lower signal attenuation) could be due to decreased diffusion from the cytotoxic edema of an acute infarct or a change in the T_2 decay (known as "T_2-shine through") (14).

Whilst the measured ADC was largely independent of the direction of the diffusion gradients in grey matter, the same was not true in white matter (15). The ADC was higher when the diffusion gradients were aligned with the predominant fiber direction, reflecting water diffusing more freely along the length of an axon than perpendicular to it (*Figure 5*). This finding led to the development of diffusion tensor imaging.

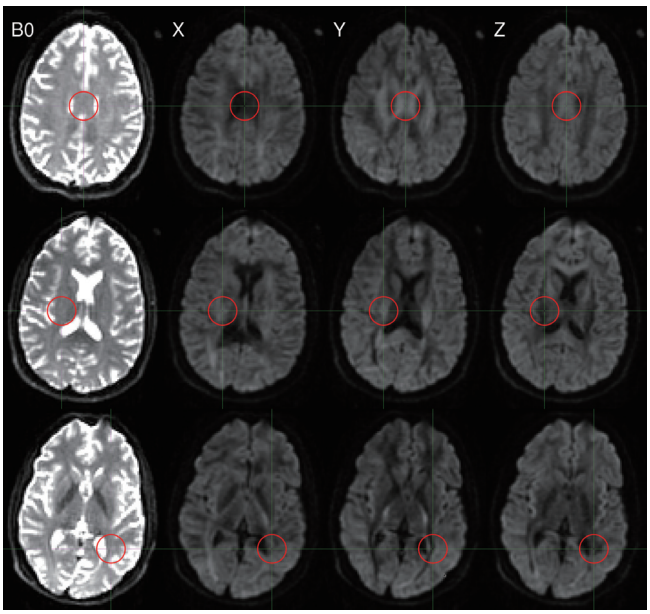

Figure 5 Diffusion-weighting imaging with gradients applied along different axes. The first column shows the non-diffusion weighted scan, the second column shows diffusion weighting applied predominantly in the x-direction (left-right), the third column the y-direction (antero-posterior) and the final column the z-direction (supero-inferior). The red circles on the first row show that signal attenuation in the corpus callosum (running left-right) is greatest with diffusion gradients in the x-direction, on the second row show the internal capsule (running supero-inferior) has greatest attenuation in the z-direction and on the third row show the optic radiation (running antero-posterior) has greatest attenuation in the y-direction

Diffusion tensor imaging (DTI)

Conceptual and mathematical formulation

Imagine a droplet of ink diffusing freely in water. Diffusion is *isotropic* as it occurs equally in all directions and a surface of constant mean-squared displacement can be represented by a *diffusion sphere* (*Figure 6*). In contrast, in many biological tissues including white matter, skeletal and cardiac muscle diffusion is anisotropic as the measured value depends on the direction. The surface of constant mean-squared displacement is then represented by a *diffusion ellipsoid* (*Figure 6*).

Anisotropic diffusion cannot be adequately represented by a single scalar ADC but can instead be represented by an effective (or apparent) diffusion tensor (16):

$$\mathbf{D} = \begin{bmatrix} D_{xx} & D_{xy} & D_{xz} \\ D_{xy} & D_{yy} & D_{yz} \\ D_{xz} & D_{yz} & D_{zz} \end{bmatrix} \quad [7]$$

The diffusion tensor is a matrix of variances and covariances that quantifies diffusion along the orthogonal axes (diagonal elements) and the correlations between these (off-diagonal elements). It is symmetric so has six independent parameters. Just as the ADC can be derived using simple linear regression and 2 DWIs, the diffusion tensor can be derived through multivariate linear regression with at least 7 DWIs along non-collinear, non-coplanar directions (17). Typically, at least one of the DWIs has negligible diffusion-weighting (b=0 image).

Equation [6] can now be generalized to incorporate the diffusion tensor ***D***. The *b*-factor is replaced by the *b*-matrix which performs the same role for anisotropic diffusion as the scalar *b*-factor does for isotropic diffusion in representing the interactions between diffusion and imaging gradients:

$$\ln\left(\frac{S(\mathbf{b})}{S(\mathbf{0})}\right) = -\sum_{i=x,y,z}\sum_{j=x,y,z} b_{ij}D_{ij} \quad [8]$$
$$= \left(-b_{xx}D_{xx} + 2b_{xy}D_{xy} + 2b_{xz}D_{xz} + b_{yy}D_{yy} + 2b_{yz}D_{yz} + b_{zz}D_{zz}\right)$$

where $S(\mathbf{b})$ is the signal in the presence of the diffusion gradients described by the symmetric *b*-matrix **b** with components b_{ij} and $S[\mathbf{0}]$ is the signal in the absence of diffusion-weighting.

In *Figure 6*, the laboratory frame of reference is [x,y,z]. However by using a frame of reference [x',y',z'] with an axis coincident with the principal axis of the diffusion ellipsoid, the off-diagonal terms become zero so the signal attenuation is:

$$\ln\left(\frac{S(\mathbf{b})}{S(\mathbf{0})}\right) = \left(-b_{x'x'}D_{x'x'} + b_{y'y'}D_{y'y'} + b_{z'z'}D_{z'z'}\right) \quad [9]$$

This frame of reference and diffusivities can be found by diagonalizing the matrix ***D*** to yield three eigenvectors and three eigenvalues. The eigenvectors give the unique local orthogonal coordinate system $[\varepsilon_1,\varepsilon_2,\varepsilon_3]$ in which displacements along orthogonal directions appear uncorrelated and whose directions correspond to the internal tissue structure. In white matter the principal eigenvector ε_1 is inferred to represent the predominant fiber orientation. The degree of diffusion along these three principles axes is given by the three eigenvalues λ_1, λ_2, λ_3 (principal diffusivities). The diffusion ellipsoid representation (*Figure 6*) has axes aligned with the eigenvectors with a magnitude proportional to the square

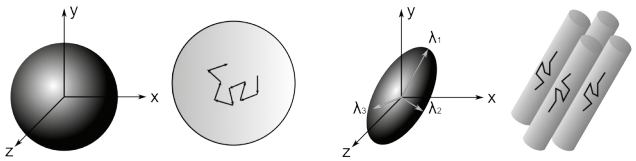

Figure 6 Diffusion sphere and ellipsoid. With isotropic diffusion, diffusion is equal in all directions and can be represented as a sphere (left) whilst anisotropic diffusion can be visualized as an ellipsoid (right)

roots of the corresponding eigenvalues.

Scalar invariants from the diffusion tensor

Scalar quantities can be derived from the eigenvalues on a voxelwise basis. These are known as "scalar invariants" as they are rotationally (and translationally) invariant and measure parameters intrinsic to the tissue. They are independent of the laboratory frame of reference, the direction of the applied imaging and diffusion-sensitizing gradients, the position of the patient and the orientation of structures contributing to the anisotropy. Distributing the gradient directions on a unit sphere according to an electrostatic energy minimization technique (18) with an acquisition including at least 30 directions (19) is necessary to reduce bias and ensure statistically rotationally-invariant reconstruction of tensor parameters.

Trace and mean diffusivity (MD)

The trace of the diffusion tensor is proportional to the orientationally averaged apparent diffusivity so removes the orientational dependence of the ADC. In clinical studies, this is typically divided by three to yield the mean diffusivity (MD). The values of MD are remarkable similar across grey and white matter, between different subjects and across mammalian species at 0.7×10^{-3} mm^2s^{-1} (*Figure* 7).

$$Trace(\mathbf{D}) = \lambda_1 + \lambda_2 + \lambda_3 \text{ and } MD(\mathbf{D}) = \frac{\lambda_1+\lambda_2+\lambda_3}{3} \quad [10]$$

Fractional anisotropy (FA) and relative anisotropy (RA)

The degree to which diffusion is anisotropic can be quantified by looking at the degree to which the diffusion tensor deviates from isotropy (20). Relative anisotropy (RA), compares the "magnitude" the anisotropic part of the diffusion tensor to the "magnitude" of the isotropic part by looking at the ratio of the variance of the eigenvalues to their mean (coefficient of variation) (21). Fractional

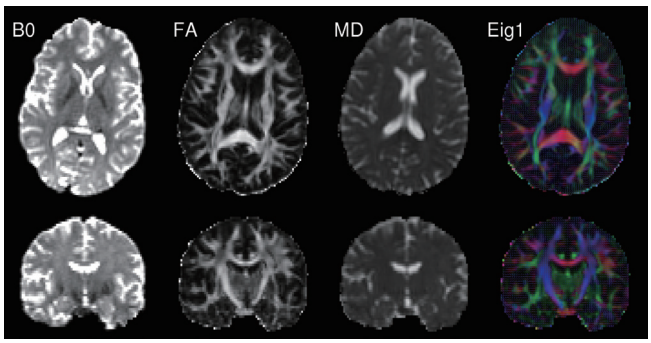

Figure 7 Diffusion tensor imaging. The non-diffusion weighted scan (B0) is shown on the left, followed by the fractional anisotropy (FA) image demonstrating higher values in white matter tracts then the mean diffusivity (MD) image with elevated values in the CSF. The final column shows the direction of principal eigenvector (Eig1) both in color-coded form (red = left/right, green=anterior/posterior, blue=superior/inferior) and in vector form (line segments)

anisotropy (FA), the more common measure, quantifies the fraction of the whole "magnitude" of the diffusion tensor that can be ascribed to anisotropic diffusion (*Figure* 7). Both include scaling coefficients to give values between 0 (isotropic diffusion) and 1 (diffusion along one axis).

$$RA(\mathbf{D}) = \sqrt{\frac{1}{3}}\frac{\sqrt{(\lambda_1-\langle D\rangle)^2+(\lambda_2-\langle D\rangle)^2+(\lambda_3-\langle D\rangle)^2}}{\langle D\rangle} = \frac{\sqrt{(\lambda_1-\lambda_2)^2+(\lambda_1-\lambda_3)^2+(\lambda_2-\lambda_3)^2}}{\lambda_1+\lambda_2+\lambda_3}$$

$$FA(\mathbf{D}) = \sqrt{\frac{3}{2}}\frac{\sqrt{(\lambda_1-\langle D\rangle)^2+(\lambda_2-\langle D\rangle)^2+(\lambda_3-\langle D\rangle)^2}}{\sqrt{\lambda_1^2+\lambda_2^2+\lambda_3^2}} = \sqrt{\frac{1}{2}}\frac{\sqrt{(\lambda_1-\lambda_2)^2+(\lambda_1-\lambda_3)^2+(\lambda_2-\lambda_3)^2}}{\sqrt{\lambda_1^2+\lambda_2^2+\lambda_3^2}} \quad [11]$$

where $\langle D\rangle = \frac{\lambda_1+\lambda_2+\lambda_3}{3}$

Decomposition of diffusion tensor components

Mean diffusivity (MD), the mean of the three eigenvalues, can be decomposed into two components, the axial (parallel, longitudinal diffusivity), $\lambda_\parallel=\lambda_1$, and the radial (perpendicular, transverse) diffusivity, $\lambda_\perp = \frac{\lambda_2+\lambda_3}{2}$ which have been considered to represent axonal and myelin integrity respectively (see below).

Similarly the diffusion tensor can be decomposed into linear, planar and spherical components (*Figure 8*)

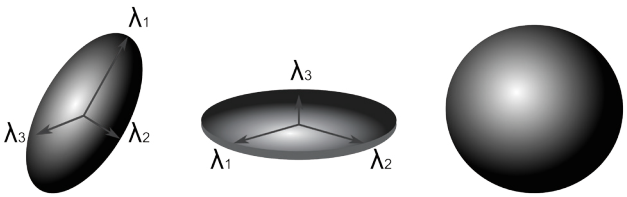

Figure 8 Diffusion ellipsoids. Linear (prolate) ellipsoid representing diffusion in one direction (left), planar (oblate) ellipsoid representing diffusion in a plane (middle) and spherical ellipsoid representing isotropic diffusion (right)

corresponding to diffusion ellipsoids that are prolate (cigar-shaped, representing diffusion in one direction, $\lambda_1 \gg \lambda_2 \simeq \lambda_3$), oblate (disc-like, representing diffusion in a plane, $\lambda_1 \simeq \lambda_2 \gg \lambda_3$) and spherical (representing isotropic diffusion, $\lambda_1 \simeq \lambda_2 \simeq \lambda_3$). By ordering the eigenvalues such that $\lambda_1 \geq \lambda_2 \geq \lambda_3 \geq 0$, the following indices (Westin metrics) may be calculated (22):

$$c_l = \frac{\lambda_1 - \lambda_2}{\lambda_1 + \lambda_2 + \lambda_3} \quad c_p = \frac{2(\lambda_1 - \lambda_2)}{\lambda_1 + \lambda_2 + \lambda_3} \quad c_s = \frac{3\lambda_3}{\lambda_1 + \lambda_2 + \lambda_3} \quad [12]$$

Each measure lies in the range 0 to 1 indicating how close the diffusion tensor is to the relative shapes and they sum to 1. A further measure describes any deviation from the spherical case, be it linear or planar anisotropy:

$$c_a = c_l + c_p = \frac{\lambda_1 + \lambda_2 - 2\lambda_3}{\lambda_1 + \lambda_2 + \lambda_3} = 1 - c_s \quad [13]$$

A second approach to the geometric shape is to assess the mode of anisotropy (23) giving a value ranging from −1 (planar anisotropic) through 0 (orthotropic) to +1 (linear anisotropic). In structures such as the corpus callosum, it is high demonstrating linear anisotropy whilst at the boundary between the corpus callosum and cingulum, it is low suggesting planar anisotropy due to crossing fibers (left-right in the corpus callosum, antero-posterior in the cingulum).

$$Mode = \frac{\lambda_1 \lambda_2 \lambda_3}{\left(\sqrt{(\lambda_1 - \langle D \rangle)^2 + (\lambda_2 - \langle D \rangle)^2 + (\lambda_3 - \langle D \rangle)^2}\right)^3} \quad [14]$$

Biological sources of diffusion anisotropy

Potential sources of anisotropy

Following the observation that diffusion is predominantly isotropic in gray matter but anisotropic in white matter (15) occurring parallel to the direction of white matter tracts (24), a key question has been the source of such anisotropy and whether it relates to a specific microstructural component. Potential contributors include the cytoskeleton (neurofilaments and microtubules), the axonal membranes and the myelin sheath (*Figure 9*). The relevant data summarized here are discussed in more detail elsewhere (25).

Myelin

The initial assumption that the relatively water impermeable lipid bilayers of the myelin sheath were the main source of diffusion anisotropy seems unlikely as myelin is not essential for anisotropy. The garfish has both myelinated and unmyelinated nerves with similar anisotropy in each (26) and diffusion anisotropy persists in genetic models of dysmyelination (27).

Myelin, although not essential, is likely to contribute to anisotropy. It is hard to study since the myelin encasing cannot be removed experimentally and a direct comparison of myelinated and unmyelinated axons is hampered by differing axonal diameters. Nevertheless, in genetic models of dysmyelination anisotropy is slightly reduced due to an increase in perpendicular diffusivity (27).

Axonal membranes

Anisotropy is present in myelinated and unmyelinated axons in the peripheral and central nervous systems in both mammalian and non-mammalian species so axonal membranes appear sufficient for anisotropy and are likely to play the primary role. In unmyelinated axons of lamprey spinal cord, anisotropy is higher in regions with more axons per cross-sectional area and thus an increased higher packing density and number of axonal membranes (28).

Cytoskeleton

Axons possess a complex internal cytoskeleton of longitudinally orientated microtubules (25 nm diameter) and neurofilaments (10 nm diameter) cross-linked with microfilaments that may present physical barriers to hinder perpendicular diffusion. Microtubules are also responsible for fast axonal transport along the length the axon which may enhance parallel diffusion.

Treatment of myelinated and unmyelinated garfish neurons with vinblastine to depolymerise and eliminate microtubules and fast axonal transport leads to a fall in both parallel and perpendicular diffusivity (which may be

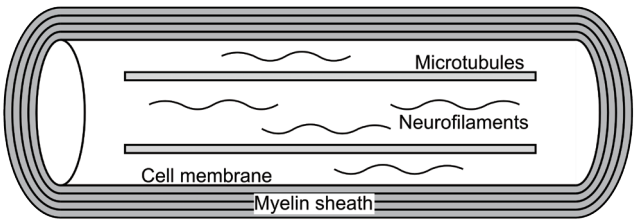

Figure 9 Possible sources of diffusion anisotropy in a myelinated nerve axon. The cytoskeleton (microtubules and neurofilaments), cell membrane and myelin sheath are all longitudinally orientated

partly an effect of time) and preservation of anisotropy (26). Similarly degradation of the microtubules (and to a lesser extent the neurofilaments) of rat optic nerve with subcutaneous methylmercury leads to an increase in parallel diffusivity but no change in perpendicular diffusivity again preserving anisotropy (29).

The contribution of the more numerous neurofilaments has been assessed with the isolated giant squid axon whose large diameter (200-1,000 μm) means the effect of the axonal membrane is insignificant with typical diffusion times. Parallel diffusivity was only around slightly greater than perpendicular diffusivity (30) and isotropic diffusion is seen in the giant reticulospinal axons of the sea lamprey spinal cord (diameter 20-40 μm) (28). The cytoskeleton does not thus appear to be a significant contributor to diffusion anisotropy.

Clinical studies of DTI parameters

Extraction of DTI parameters

For clinical studies involving DTI parameters, a suitable parameter must be extracted, compared between groups and properly interpreted. Two common techniques are employed to extract the parameter (31,32).

Voxel-based analyses take quantitative maps (e.g., FA) which are then spatially normalized to a template using non-linear registration. Following smoothing, a voxel-based comparison is undertaken between groups using software such as SPM. The main advantages of this technique are that it is automated and performs a whole brain analysis without any *a priori* hypothesis. However, sensitivity is limited by the accuracy of spatial normalization (31) and results may vary depending on the degree of smoothing (33). Statistical correction is also required for the multiple comparisons.

A variant of this technique known as Tract-Based Spatial Statistics (TBSS) determines a white matter skeleton representing the 'core' of the tracts from the group and projects each subject's FA map onto this skeleton (*Figure 10*) (34). This aims to alleviate the problems of inaccurate image registration and requires no smoothing and is widely used. It does however limit the analysis to the core of white matter so cannot detect changes occurring in the periphery of white matter tracts (or in grey matter).

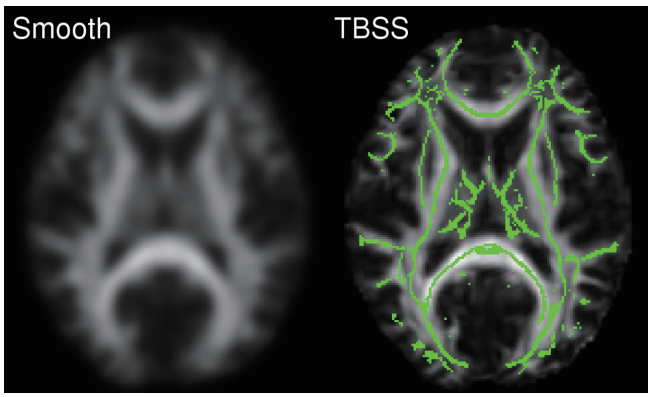

Figure 10 Voxel-based techniques for analyzing DTI parameters. In conventional voxel-based analyses the FA map is non-linearly registered to a template and smoothed (left). In Tract-Based Spatial Statistics following normalization the FA map is projected onto a white matter skeleton (right, in green).

The second main approach is region-of-interest based analysis. The structure(s) of interest are delineated either manually by an operator or automatically from an atlas and the mean of a diffusion parameter (e.g., FA) is determined in each structure in each subject. This requires an *a priori* hypothesis of which structures to assess but the single number derived per subject allows correlational analyses with clinical variables, such as cognitive scores. It cannot detect localized changes within structures, and the delineation of the structure can be time consuming and not necessarily accurate. In particular due to the relatively large voxel size of DTI, it can be hard to delineate a structure accurately and avoid partial volume effects.

Interpretation of DTI parameters

Having extracted a parameter and performed a group comparison, any differences must be interpreted. Since FA is higher in ordered white matter and typically falls in disease processes, it is often considered a direct marker of white matter integrity but this is an over-simplification (1).

FA is related to many factors including axonal count and density, degree of myelination and fiber organization. Whilst changes are frequently attributed to one or more of these factors, DTI alone cannot distinguish them and is thus non-specific. In post-mortem multiple sclerosis (MS) brains, FA positively correlated with axonal count and myelin content and negatively with degree of gliosis (35). In temporal lobe epilepsy surgery, FA of the fimbria-fornix correlated mostly strongly with the total axon membrane circumference on electron microscopy but also to a lesser extent with axonal density and myelin thickness (36).

Another critical factor is crossing fibers as two obliquely orientated fiber populations will have a lower FA than a single coherent fiber population (*Figure 11*) and thus selective loss of one of these populations will lead to a paradoxical increase in FA. This has been postulated in mild cognitive impairment with an increased FA in the centrum semiovale being related to a relative preservation of motor-related projection fibers crossing association fibers of the superior longitudinal fasciculus (37). This was supported by an increase in mode of anisotropy suggesting more linear anisotropy (see below).

MD is considered less often as it is a less sensitive measure which may rise in pathology. In the same two studies as above, opposite correlations to FA were seen in post-mortem MS brains (35) with no correlations seen in the fimbriae-fornix in epilepsy surgery (36). It is however useful to consider the separate components of diffusivity as a reduction in anisotropy may result from increased perpendicular diffusivity, decreased parallel diffusivity or a combination of the two, each of which has a different structural interpretation. In particular it may be helpful to know the specific relationship between myelin loss, axonal damage and diffusivities in conditions such as MS.

This was first addressed in animal studies. In the shiverer mouse, a genetic model of dysmyelination, perpendicular diffusivity is increased with no change in parallel diffusivity (38). In a mouse model of retinal ischemia, an early reduced parallel diffusivity with axonal degeneration on immunohistochemistry was followed by a later increased perpendicular diffusivity with myelin degradation (39). Similarly in cuprizone-induced corpus callosal damage in mice, the initial axonal damage is accompanied by reduced parallel diffusivity with later demyelination associated with increased perpendicular diffusivity (40).

Taken together these animal studies have led to the suggestion that parallel diffusivity is a marker of axonal damage whilst perpendicular diffusivity reflects myelin damage. Such an interpretation has been extended to human studies. In a study of patients with epilepsy undergoing corpus callosotomy, an early reduction in parallel diffusivity (at 1 week) was inferred to reflect axonal fragmentation with the later increase in perpendicular diffusivity (at 2-4 months) consistent with myelin degradation (41). However, these parameters may not portray an accurate reflection of demyelination especially in areas of low anisotropy due to complex tissue architecture such as crossing fibers (42).

Finally the geometrical diffusion anisotropy indices - linear, planar and spherical anisotropy and mode of anisotropy - have been less widely used but may give an indication of the geometrical structure of tissue. In a rat model of glioma, high c_p around the tumor was found to be associated with compression of cells perpendicular to the tumor surface thus making them more planar (43). A similar rim of high c_p has been seen in humans around glioblastoma multiforme with higher FA and c_l inside the tumor than metastases (44). Likewise increased FA and c_p seen within epidermoid cysts suggesting planar diffusion may reflect the highly parallel-layered arrangement of keratin filaments within tumor (45). Mode of anisotropy may also help in assessing the effect of crossing fibers on FA values with planar anisotropy suggesting crossing fibers and linear anisotropy suggesting a single fiber (37).

Fiber orientation and tractography

The diffusion tensor model assumes that the direction of the principal eigenvector ε_1 in each voxel is aligned with the predominant direction of fibers locally. The eigenvectors can be displayed either as a vector field or through color coding (*Figure* 7). The Directionally Encoded Color (DEC) scheme represents the x, y and z components in red, green and blue respectively (46) so fibers running left-right are red, antero-posterior green and supero-inferior blue. However unlike the scalar indices above, color coding is orientationally variant.

Tractography is the process by which white matter connections are inferred by tracing through these vector fields (*Figure 12*). The resulting tracts may be used qualitatively for surgical planning, or quantitative parameters may be extracted. These include the volume of connections and fiber counts which have significant limitations (1) or an assessment of the degree of connectivity or connection strength between different regions. These parameters are not reviewed here but it is worth noting that

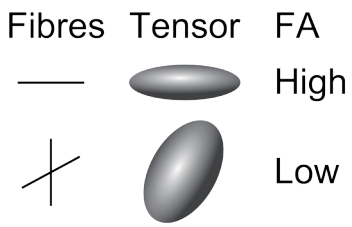

Figure 11 The problem with FA and crossing fibers. With a single fiber population, the diffusion tensor is prolate so FA is high. With two fiber populations crossing at 60 degrees, the diffusion tensor becomes more oblate so the FA is reduced

the delineated tract can also provide a region-of-interest for the DTI parameters discussed above.

Improving the diffusion model

Limitations of diffusion tensor model

Whilst the diffusion tensor model provides helpful quantitative parameters, it is based on the fundamental assumption that within each voxel there is a single diffusing process that follows a Gaussian distribution. Studies have shown that with higher *b*-values the measured diffusion signal deviates from the linear relationship predicted by equation 6 so the assumption of Gaussian diffusion is not valid (47).

The diffusion signal from a single voxel reflects the contribution of several tissue compartments with differing diffusion profiles. Further the large voxel size in diffusion imaging (typically 2 mm isotropic) in comparison to underlying microstructure means that a single voxel may contain a mixture of grey matter, white matter and cerebrospinal fluid (partial voluming effect) and even within white matter, a voxel may contain a variety of fiber populations with different orientations. Thus in white matter with complex fiber architectures (crossing or diverging fibers) or in grey matter where diffusion is relatively isotropic this model fits poorly (48).

Diffusion profile

The diffusion profile within a voxel can be more accurately measured by acquiring data with increased angular resolution (HARDI, high angular resolution diffusion imaging) (49), with varying *b*-values to assess the deviation from Gaussian diffusion or a combination of the two. The spatial diffusion profile obtained, the diffusion orientation distribution function (dODF), reflects the relative amount

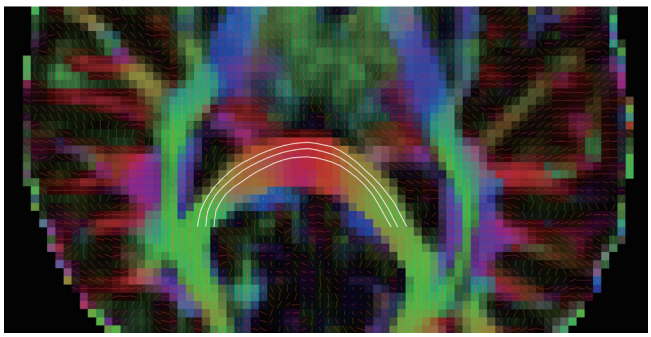

Figure 12 Principle of tractography. Close up of the corpus callosum with the vector field from the principal eigenvectors and white lines indicating how tractography algorithms follow the vector field

of diffusion in different directions.

These data may be acquired and assessed using model-free approaches such as Q-ball imaging (50) or diffusion spectrum imaging (51) which make no assumptions on the underlying diffusion profile but these do not give immediate quantitative values and are not discussed further. A second approach is to design a biologically plausible model of the tissue and relate parameters of this model such as axonal density to the measured diffusion signal (52). If the model is valid, by fitting the model to the measured diffusion data these quantitative parameters may be extracted. Some examples of such models are now given.

Tissue models

The bi-exponential model addresses the discrepancy with higher *b*-values by considering two different diffusing pools (fast and slow) with separate diffusion coefficients and volume fractions (47). Whilst this model fits well, the fast and slow decaying components are not equivalent to the extra- and intracellular components as originally hypothesized as the fitted volume fractions are significantly different. This model does not allow for exchange between the compartments and with increasing *b*-values, the fit requires higher order exponentials (53).

The ball-and-stick model consists of an intra-axonal fraction modeled as a "stick" (idealized cylinder with zero radius) and an extra-axonal fraction modeled as a "ball" (isotropic diffusion) (54). This formulation allows an estimate of fiber orientation, the relative volume fraction of the two components and their associated diffusion coefficients. The model can be extended to multiple fibers

and is implemented in FSL for tractography (55).

The CHARMED (Composite Hindered and Restricted Model of Diffusion) model encompasses the different forms of diffusion in biological systems (56). Intra-axonal diffusion is *restricted* due to barriers such as the cell membrane resulting in non-Gaussian diffusion with increasing diffusion time. It is modeled as impermeable parallel cylinders of a given diameter and can be extended to cover multiple fiber orientations. Extra-axonal diffusion is *hindered* due to obstacles increasing the mean path length between positions, characterized by the degree of tortuosity and is modeled by a diffusion tensor (anisotropic Gaussian diffusion). Fitted parameters give estimates of the diffusivity in the extra-axonal matrix (diffusivity of hindered part), the axonal density (volume fraction of the restricted part) and fiber orientations (ODF of the restricted part).

AxCaliber extends this framework to replace the fixed axon diameter by a gamma distribution to allow the axon diameter distribution to be estimated (57). However to achieve a realistic scan time, diffusion was only measured perpendicular to the long axis of the nerve so must be known in advance (for example the corpus callosum) and the estimates obtained deviate from histological findings.

More recently two key factors that affect FA, neurite density and fiber orientation dispersion, have been estimated within a clinically feasible scan duration (20 minutes) using NODDI (neurite orientation dispersion and density imaging) (58). This relaxes the constraint of the above models which assume parallel cylinders and allows dispersion of fiber orientation. It employs a three-compartment model with the intra-cellular compartment modeled by "sticks" (cylinders of zero radius) with orientation dispersion represented by a Watson distribution, the extra-cellular compartment as Gaussian anisotropic diffusion and the CSF compartment as Gaussian isotropic diffusion.

Limitations of models

Models with additional parameters require a longer acquisition to provide the necessary data to perform the fitting so there is always a balance between the accuracy of the model and the acquisition time. By incorporating various assumptions to reduce the number of free parameters scan time is reduced at the expense of the accuracy of the model. In general a combination of the low spatial resolution, poor signal-to-noise with higher *b*-values and the necessary length of acquisition limit their clinical utility (52) although NODDI does represent a clinically feasible scan. These techniques need further assessment before routine clinical use.

Conclusions

Diffusion is a fundamental physical process characterized by the diffusion coefficient that can be quantified with diffusion MRI. Diffusion-weighted imaging measures the apparent diffusion coefficient which incorporates the effect of barriers on free diffusion and other factors such as perfusion and is useful in detecting early ischemia. However diffusion in biological tissues is fundamentally anisotropic which is better represented mathematically by a diffusion tensor.

Diagonalization of this diffusion tensor provides eigenvectors, the orthogonal axes of diffusion used for tractography, and eigenvalues, a measure of diffusivity along these axes. Scalar invariants derived from the eigenvalues including FA and MD provide sensitive but non-specific measures of pathology that may be affected by a numerous factors.

The diffusion tensor remains widely used but increasingly its limitations are being recognized. The assumption of a single compartment with Gaussian diffusion does not adequately model biological systems. By fitting biologically plausible models of white matter to the diffusion profile, additional parameters such as axonal density, axonal diameter distributions and fiber orientations may be derived. These techniques hold promise to provide more quantitative parameters via diffusion MRI but are not yet in widespread clinical use due in part to lengthy acquisition times.

Acknowledgements

Gavin Winston was supported by a Clinical Research Training Fellowship from the Medical Research Council (G0802012). The Big Lottery Fund, Wolfson Trust and the Epilepsy Society support the Epilepsy Society MRI scanner on which the example scans were acquired. This work was undertaken at UCLH/UCL who received a proportion of funding from the Department of Health's NIHR Biomedical Research Centres funding scheme.
Disclosure: The authors declare no conflict of interest.

References

1. Jones DK, Knösche TR, Turner R. White matter integrity, fiber count, and other fallacies: The do's and don'ts of

diffusion MRI. Neuroimage 2012. [Epub ahead of print]
2. Fick A. Über Diffusion. Ann Phys 1855;94:59.
3. Einstein A. Über die von der molekularkinetischewn Theorie der wärme gefordete Bewegung von in ruhenden Flüssigkeiten suspendierten Teilchen. Ann Physik 1905;4:549-60.
4. Hahn EL. Spin echoes. Phys Rev 1950;80:580-94.
5. Stejskal EO, Tanner JE. Spin diffusion measurements: spin echoes in the presence of time-dependent field gradient. J Chem Phys 1965;42:288-92.
6. Torrey HC. Bloch equations with diffusion terms. Phys Rev 1956;104:563-5.
7. Turner R, Le Bihan D, Chesnick AS. Echo-planar imaging of diffusion and perfusion. Magn Reson Med 1991;19:247-53.
8. Basser PJ, Jones DK. Diffusion-tensor MRI: theory, experimental design and data analysis - a technical review. NMR Biomed 2002;15:456-67.
9. Bammer R. Basic principles of diffusion-weighted imaging. Eur J Radiol 2003;45:169-84.
10. Le Bihan D. Molecular diffusion nuclear magnetic resonance imaging. Magn Reson Q 1991;7:1-30.
11. Le Bihan D, Breton E, Lallemand D, et al. MR imaging of intravoxel incoherent motions: application to diffusion and perfusion in neurologic disorders. Radiology 1986;161:401-7.
12. Moseley ME, Cohen Y, Mintorovitch J, et al. Early detection of regional cerebral ischemia in cats: comparison of diffusion- and T2-weighted MRI and spectroscopy. Magn Reson Med 1990;14:330-46.
13. Warach S, Chien D, Li W, et al. Fast magnetic resonance diffusion-weighted imaging of acute human stroke. Neurology 1992;42:1717-23.
14. Burdette JH, Elster AD, Ricci PE. Acute cerebral infarction: quantification of spin-density and T2 shine-through phenomena on diffusion-weighted MR images. Radiology 1999;212:333-9.
15. Moseley ME, Cohen Y, Kucharczyk J, et al. Diffusion-weighted MR imaging of anisotropic water diffusion in cat central nervous system. Radiology 1990;176:439-45.
16. Basser PJ, Mattiello J, LeBihan D. Estimation of the effective self-diffusion tensor from the NMR spin echo J Magn Reson B 1994;103:247-54.
17. Basser PJ, Pierpaoli C. A simplified method to measure the diffusion tensor from seven MR images. Magn Reson Med 1998;39:928-34.
18. Jones DK, Horsfield MA, Simmons A. Optimal strategies for measuring diffusion in anisotropic systems by magnetic resonance imaging. Magn Reson Med 1999;42:515-25.
19. Jones DK. The effect of gradient sampling schemes on measures derived from diffusion tensor MRI: a Monte Carlo study. Magn Reson Med 2004;51:807-15.
20. Pierpaoli C, Basser PJ. Toward a quantitative assessment of diffusion anisotropy. Magn Reson Med 1996;36:893-906.
21. Basser PJ, Pierpaoli C. Microstructural and physiological features of tissues elucidated by quantitative-diffusion-tensor MRI. J Magn Reson B 1996;111:209-19.
22. Westin CF, Peled S, Gudbjartsson H, et al. Geometrical diffusion measures for MRI from tensor basis analysis. Proceedings of the 5th Annual Meeting of ISMRM. Vancouver, Canada, 1997;1742.
23. Ennis DB, Kindlmann G. Orthogonal tensor invariants and the analysis of diffusion tensor magnetic resonance images. Magn Reson Med 2006;55:136-46.
24. Moseley ME, Kucharczyk J, Asgari HS, et al. Anisotropy in diffusion-weighted MRI. Magn Reson Med 1991;19:321-6.
25. Beaulieu C. The basis of anisotropic water diffusion in the nervous system - a technical review. NMR Biomed 2002;15:435-55.
26. Beaulieu C, Allen PS. Determinants of anisotropic water diffusion in nerves. Magn Reson Med 1994;31:394-400.
27. Gulani V, Webb AG, Duncan ID, et al. Apparent diffusion tensor measurements in myelin-deficient rat spinal cords. Magn Reson Med 2001;45:191-5.
28. Takahashi M, Hackney DB, Zhang G, et al. Magnetic resonance microimaging of intraaxonal water diffusion in live excised lamprey spinal cord. Proc Natl Acad Sci U S A 2002;99:16192-6.
29. Kinoshita Y, Ohnishi A, Kohshi K, et al. Apparent diffusion coefficient on rat brain and nerves intoxicated with methylmercury. Environ Res 1999;80:348-54.
30. Beaulieu C, Allen PS. Water diffusion in the giant axon of the squid: implications for diffusion-weighted MRI of the nervous system. Magn Reson Med 1994;32:579-83.
31. Snook L, Plewes C, Beaulieu C. Voxel based versus region of interest analysis in diffusion tensor imaging of neurodevelopment. Neuroimage 2007;34:243-52.
32. Chanraud S, Zahr N, Sullivan EV, et al. MR diffusion tensor imaging: a window into white matter integrity of the working brain. Neuropsychol Rev 2010;20:209-25.
33. Jones DK, Symms MR, Cercignani M, et al. The effect of filter size on VBM analyses of DT-MRI data. Neuroimage 2005;26:546-54.
34. Smith SM, Jenkinson M, Johansen-Berg H, et al. Tract-based spatial statistics: voxelwise analysis of multi-subject diffusion data. Neuroimage 2006;31:1487-505.
35. Schmierer K, Wheeler-Kingshott CA, Tozer DJ, et al.

Quantitative magnetic resonance of postmortem multiple sclerosis brain before and after fixation. Magn Reson Med 2008;59:268-77.
36. Concha L, Livy DJ, Beaulieu C, et al. In vivo diffusion tensor imaging and histopathology of the fimbria-fornix in temporal lobe epilepsy. J Neurosci 2010;30:996-1002.
37. Douaud G, Jbabdi S, Behrens TE, et al. DTI measures in crossing-fibre areas: increased diffusion anisotropy reveals early white matter alteration in MCI and mild Alzheimer's disease. Neuroimage 2011;55:880-90.
38. Song SK, Sun SW, Ramsbottom MJ, et al. Dysmyelination revealed through MRI as increased radial (but unchanged axial) diffusion of water. Neuroimage 2002;17:1429-36.
39. Song SK, Sun SW, Ju WK, et al. Diffusion tensor imaging detects and differentiates axon and myelin degeneration in mouse optic nerve after retinal ischemia. Neuroimage 2003;20:1714-22.
40. Sun SW, Liang HF, Trinkaus K, et al. Noninvasive detection of cuprizone induced axonal damage and demyelination in the mouse corpus callosum. Magn Reson Med 2006;55:302-8.
41. Concha L, Gross DW, Wheatley BM, et al. Diffusion tensor imaging of time-dependent axonal and myelin degradation after corpus callosotomy in epilepsy patients. Neuroimage 2006;32:1090-9.
42. Wheeler-Kingshott CA, Cercignani M. About "axial" and "radial" diffusivities. Magn Reson Med 2009;61:1255-60.
43. Kim S, Pickup S, Hsu O, et al. Diffusion tensor MRI in rat models of invasive and well-demarcated brain tumors. NMR Biomed 2008;21:208-16.
44. Wang S, Kim S, Chawla S, et al. Differentiation between glioblastomas and solitary brain metastases using diffusion tensor imaging. Neuroimage 2009;44:653-60.
45. Jolapara M, Kesavadas C, Radhakrishnan VV, et al. Diffusion tensor mode in imaging of intracranial epidermoid cysts: one step ahead of fractional anisotropy. Neuroradiology 2009;51:123-9.
46. Pajevic S, Pierpaoli C. Color schemes to represent the orientation of anisotropic tissues from diffusion tensor data: application to white matter fiber tract mapping in the human brain. Magn Reson Med 1999;42:526-40.
47. Niendorf T, Dijkhuizen RM, Norris DG, et al. Biexponential diffusion attenuation in various states of brain tissue: implications for diffusion-weighted imaging. Magn Reson Med 1996;36:847-57.
48. Tuch DS, Reese TG, Wiegell MR, et al. High angular resolution diffusion imaging reveals intravoxel white matter fiber heterogeneity. Magn Reson Med 2002;48:577-82.
49. Frank LR. Characterization of anisotropy in high angular resolution diffusion-weighted MRI. Magn Reson Med 2002;47:1083-99.
50. Tuch DS. Q-ball imaging. Magn Reson Med 2004;52:1358-72.
51. Wedeen VJ, Hagmann P, Tseng WY, et al. Mapping complex tissue architecture with diffusion spectrum magnetic resonance imaging. Magn Reson Med 2005;54:1377-86.
52. Panagiotaki E, Schneider T, Siow B, et al. Compartment models of the diffusion MR signal in brain white matter: a taxonomy and comparison. Neuroimage 2012;59:2241-54.
53. Assaf Y, Cohen Y. Non-mono-exponential attenuation of water and N-acetyl aspartate signals due to diffusion in brain tissue. J Magn Reson 1998;131:69-85.
54. Behrens TE, Woolrich MW, Jenkinson M, et al. Characterization and propagation of uncertainty in diffusion-weighted MR imaging. Magn Reson Med 2003;50:1077-88.
55. Behrens TE, Berg HJ, Jbabdi S, et al. Probabilistic diffusion tractography with multiple fibre orientations: What can we gain? Neuroimage 2007;34:144-55.
56. Assaf Y, Basser PJ. Composite hindered and restricted model of diffusion (CHARMED) MR imaging of the human brain. Neuroimage 2005;27:48-58.
57. Assaf Y, Blumenfeld-Katzir T, Yovel Y, et al. AxCaliber: a method for measuring axon diameter distribution from diffusion MRI. Magn Reson Med 2008;59:1347-54.
58. Zhang H, Schneider T, Wheeler-Kingshott CA, et al. NODDI: practical in vivo neurite orientation dispersion and density imaging of the human brain. Neuroimage 2012;61:1000-16.

Cite this article as: Winston GP. The physical and biological basis of quantitative parameters derived from diffusion MRI. Quant Imaging Med Surg 2012;2(4):254-265. DOI: 10.3978/j.issn.2223-4292.2012.12.05

